tained and noting accuracy of the individual measurements, we arrive at a value of $k=-162\pm16$.

Thus, almost within the known experimental errors of the various measurements, the dynamic nuclear polarization of ANI can be computed from the modified Bloch equation [Eq. (1)] with $T_1=T_2=50$ nsec and the Solomon relation [Eq. (6)] with $k=-162$ over a wide range of fields and under resonant and nonresonant conditions.

Some unexplained behavior was noted in an ANI sample which had deteriorated over a period of time. The time constant for the establishment of the steady-state dynamic nuclear polarization varied markedly with H_{rf} and was, in addition, much longer than T_1 for the proton spin system. It has been reported,[12] without knowledge of the sample deterioration, that this system did not respond according to both Eqs. (1) and (6), but this has now been attributed to sample deterioration.

One of the other solutions on which the low-field dynamic nuclear polarization measurements were made was a free-radical derived from crude oil, which was studied by Poindexter.[11] This particular radical is *not* exchange-narrowed, and its linewidth is hyperfine broadened. For it, $T_1>T_2\cong10$ nsec. Large signals were obtained from this solution with $H_0=0.5$ G as well.

A check was made of the effect of direction of the rf field. The coils producing H_{rf} were turned parallel to the dc field H_0. The ANI solution yielded absolutely no detectable "parallel" signal under conditions where the perpendicular fields gave a signal-to-noise ratio of nearly 50. This was expected from the MBE. However, Poindexter's radical solution yielded a "parallel" signal approximately one-third as large as the "perpendicular." We believe that this is due to the existence of unresolved hyperfine states in the radical, which would permit electron absorption between $m_F=0$ components, where m_F is the total electron-plus-nucleus spin magnetic quantum number. These transitions are known to have parallel transition probabilities in weak dc fields.

We believe this transient dynamic nuclear polarization technique to be a very useful way to study electron relaxation behavior of solutions. First, large values of H_{rf} may be obtained at these low frequencies with conventional amateur transmitters; and second, the transient method avoids the troublesome rf heating problems encountered in continuous wave experiments. The rf is applied for only about 1 sec to fully polarize the nuclei.

[12] R. J. S. Brown and Don D. Thompson, Bull. Am. Phys. Soc. 8, 620 (1963).

PHYSICAL REVIEW VOLUME 136, NUMBER 5A 30 NOVEMBER 1964

Transverse and Longitudinal Optic Mode Study in MgF_2 and ZnF_2

A. S. Barker, Jr.
Bell Telephone Laboratories, Murray Hill, New Jersey
(Received 2 July 1964)

Infrared reflectivity measurements have been made on single-crystal MgF_2 and ZnF_2 in the wavelength range 1 to 140 μ. An analysis of the data using Kramers–Kronig analysis and classical dispersion theory gives the transverse optic mode frequencies, strengths, and linewidths. Huang's macroscopic dielectric theory is extended to the case of several modes to study the behavior of the longitudinal optic modes in these fluorides. A generalized Lyddane-Sachs-Teller relation and some additional sum rules are derived for the case of many modes when damping is present. It is shown that the longitudinal mode frequencies are easily obtainable from the reflectivity data analysis. The four longitudinal optic mode frequencies for MgF_2 and ZnF_2 are presented.

INTRODUCTION

MAGNESIUM fluoride and zinc fluoride are optically transparent insulators which crystallize with the rutile structure. This structure has space group $P4_2/mnm$ and point group D_{4h}. A group character analysis shows that these materials should exhibit three doubly degenerate infrared active modes with the electric vector perpendicular to the c axis and one nondegenerate infrared active mode with the electric vector parallel to the c axis.[1] At the present time the frequencies of these modes have not been established. A recent report by Hunt *et al.* describes reflection experiments done on polycrystalline MgF_2.[2] Since reflectivity is a nonlinear function of the dielectric constant, analysis of average reflectivity does not yield an average dielectric constant for noncubic crystals. Thus the analysis carried out by Hunt *et al.* yields some incorrect frequencies and mode symmetries. Recent experiments performed by Johnson *et al.* on nickel- and cobalt-doped MgF_2[3,4] and cobalt-doped ZnF_2 have

[1] P. S. Narayanan, J. Indian Acad. Sci. 32A, 279 (1950).

[2] G. R. Hunt, C. H. Perry, and J. Ferguson, Phys. Rev. 134, A688 (1964).

[3] L. F. Johnson, R. E. Dietz, and H. J. Guggenheim, Phys. Rev. Letters 11, 318 (1963).

[4] L. F. Johnson, R. E. Dietz, and H. J. Guggenheim (to be published).

shown that phonon-terminated laser action is possible. In MgF_2:Ni the characteristic phonon frequencies are 340 cm^{-1}. In ZnF_2:Co there is some ambiguity in the assignment of the phonon energy, the most likely assignments being in the range 380 to 540 cm^{-1}. The present work is a study of the phonon properties of MgF_2 and ZnF_2 which can be detected by infrared techniques. Polarized reflection spectra are taken from suitably oriented samples to give the mode structure of the infrared active vibrations. Analysis of the real part of the dielectric constant gives the longitudinal optic (inactive) vibration frequencies. Huang's theory of the long-wave optic vibrations is extended to the multimode case to illustrate the longitudinal mode effects and to derive a general Lyddane-Sachs-Teller relation in the case of many modes with velocity-dependent damping.

EXPERIMENTAL

Two single-crystal samples of MgF_2 were oriented by x-ray then cut and polished by usual metallographic

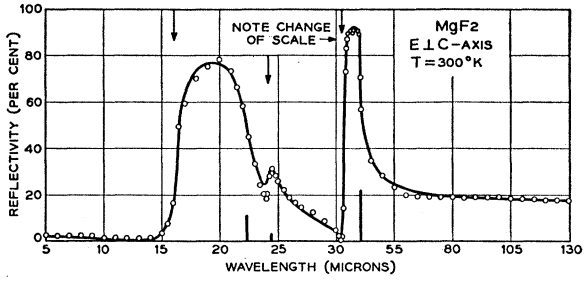

FIG. 1. Reflectivity of MgF_2 for the electric vector of the infrared beam perpendicular to the c axis. The solid curve is the best fit obtained using classical oscillator dispersion theory. The solid bars show the transverse mode frequencies and strengths. A mode strength of 1.0 is given an ordinate of 10% reflectivity. The arrows give the longitudinal mode frequencies.

techniques. One sample contained about 1% Ni and 1% Co and had a pink-orange color. The second sample contained about 0.5% Ni and was optically clear. A small boule of ZnF_2 doped with about 1% cobalt was oriented by using Laue x-ray photographs. A rectangular sample 3.5 by 4.2 by 11.0 mm was cut from the boule so that the c axis was parallel to the 3.5-mm edge. The sample had a deep red color. All samples showed symmetric, clearly defined optic figures when examined with crossed polariods. Room temperature reflection spectra were taken in the range 1 to 140 μ for the electric vector E of the infrared beam perpendicular to the c axis. Conventional pile of plates polarizers were used.[5] In the $E\|c$-axis configuration all samples had somewhat smaller surface areas, and measurements could be carried out only to about 45 μ because of the limited energy available. In all experiments the angle of

[5] W. G. Spitzer and D. A. Kleinman, Phys. Rev. **121**, 1324 (1961).

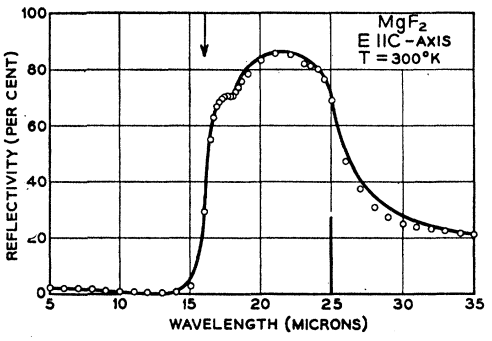

FIG. 2. Reflectivity of MgF_2 for E parallel to the c axis. The solid curve is given by the classical oscillator dispersion theory with one strong mode and one weak (forbidden) mode.

incidence was near 15°. For both materials the wavelength range was sufficient to cover completely the restrahlen band structure which was found. The types of spectrometers and the measurement techniques have been described previously.[5,6] The measured reflectivities are shown by the points in Figs. 1–4. For MgF_2 where two samples were studied, no features of the spectrum could be associated with the nickel and cobalt doping.

DISCUSSION

It is useful when presenting infrared lattice vibration data to characterize the modes by their strengths, frequencies and linewidths. This is most easily done using the classical oscillator dispersion theory where these parameters appear explicitly and can be determined by a curve-fitting procedure. In applying the dispersion theory to tetragonal crystals, it is assumed that the dielectric behavior of the crystal can be described by two dielectric functions, one for $E\perp c$ axis and one for $E\|$ c axis. The parameters entering these functions are a strength, frequency, and linewidth for each mode and an asymptotic value for the dielectric constant at high frequencies. Values for the parameters are chosen so that the dielectric functions correctly predict the measured infrared reflectivity. The fitting technique has been discussed extensively in the liter-

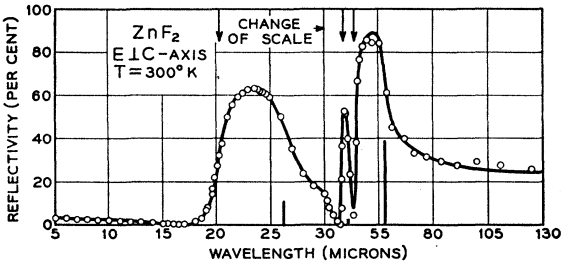

FIG. 3. Reflectivity of ZnF_2 for E perpendicular to the c axis. The solid curve is given by the classical oscillator dispersion theory. Transverse and longitudinal phonon modes are indicated by vertical bars and arrows.

[6] A. S. Barker, Jr., Phys. Rev. **132**, 1474 (1963).

TABLE I. Infrared phonon parameters for MgF_2 and ZnF_2.

Frequency (cm^{-1})	Wavelength (μ)	Strength S_j	Linewidth γ_j/ω_j	Limiting dielectric constants
	MgF_2 $E\perp c$ axis (symmetry type E_u)			
247	40.6	2.22	0.014	$\epsilon_\infty=1.9$
410	24.4	0.19	0.033	$\epsilon_0=5.4$
450	22.2	1.14	0.058	
303	33.0	(longitudinal mode)[c]		
415	24.1	(longitudinal mode)		
617	16.2	(longitudinal mode)		
	MgF_2 $E\parallel c$ axis (symmetry type A_{2u})			
399	25.0	2.7	0.048	$\epsilon_\infty=1.9$
556[a]	18.0	0.01	0.08	$\epsilon_0=4.6$
625	16.0	(longitudinal mode)		
	ZnF_2 $E\perp c$ axis (symmetry type E_u)			
173	57.8	4.0	0.035	$\epsilon_\infty=2.1$
244	41.0	0.24	0.037	$\epsilon_0=7.5$
380	26.3	1.13	0.088	
227	44.1	(longitudinal mode)		
264	37.9	(longitudinal mode)		
498	20.1	(longitudinal mode)		
	ZnF_2 $E\parallel c$ axis (symmetry type A_{2u})			
294	34.0	4.6	0.092	$\epsilon_\infty\sim2.6$[b]
488	20.5	(longitudinal mode)		$\epsilon_0=7.2$

[a] Weak forbidden mode.
[b] The high-frequency reflectivity did not approach a constant value causing about 10% uncertainty for ϵ_∞.
[c] The effective charges and damping coefficients for the longitudinal vibrations can be obtained by transforming to new longitudinal mode amplitudes W_j' which diagonalize the force constant matrix for longitudinal motions. These longitudinal charges may be of interest since they determine the polaron coupling constants.

ature.[5,7] The solid curves in Figs. 1–4 show the fits that have been obtained with the dispersion theory. The corresponding mode parameters are given in Table I. In addition to the infrared active phonon frequencies (which correspond to transverse optic vibrations), the longitudinal optic phonon frequencies may also be obtained from the dispersion theory. Before discussing the longitudinal optic mode frequencies, it seems desirable to present a simple theory to illustrate the behavior and significance of the longitudinal vibrations.

MACROSCOPIC LATTICE VIBRATION MODEL

Huang has given a macroscopic model for the dielectric behavior of a crystal with one infrared active mode.[8] He has shown that this model can arise from the microscopic equation of motion of the ions in an NaCl-type lattice including electronic polarizability and internal electric field effects. Since the effective charges, electronic polarizabilities, and local fields are not known for most noncubic crystals, we will start in the present work with simple macroscopic equations extended to several modes. Taking W_j to be the vibration amplitude of the jth optic mode,[9] we write

$$\begin{aligned}&\ddot{W}_1+\omega_1^2W_1+\gamma_1\dot{W}_1=Z_1E,\\&\ddot{W}_2+\omega_2^2W_2+\gamma_2\dot{W}_2=Z_2E,\ \cdots,\\&\ddot{W}_n+\omega_n^2W_n+\gamma_n\dot{W}_n=Z_nE.\end{aligned}\tag{1}$$

The ω_j^2, γ_j, and Z_j are the restoring force, damping coefficient, and effective charge coefficients respectively of the jth mode. The damping terms are of the usual velocity-dependent type introduced in a rather *ad hoc* manner for simplicity.[10] It must be emphasized that the restoring force and effective charge coefficients are not directly related to the microscopic forces and charges because of local field effects. E is the macroscopic electric field in the crystal. We take the polarization of the crystal to be

$$P=\alpha_1W_1+\alpha_2W_2+\cdots+\alpha_nW_n+\alpha_\infty E.\tag{2}$$

Here also, local field effects prevent identification of the α_j with the effective charge per unit volume.[11] α_∞ describes the very high-frequency behavior due to electronic effects. At very high frequencies the ions can no longer follow the motion so $W_j=0$ leaving the dielectric behavior completely determined by α_∞. We restrict ourselves to plane waves whose wave vector and polarization vector lie along principal crystal directions allowing scalar equations to be written. For tetragonal crystals, therefore, we have two sets of

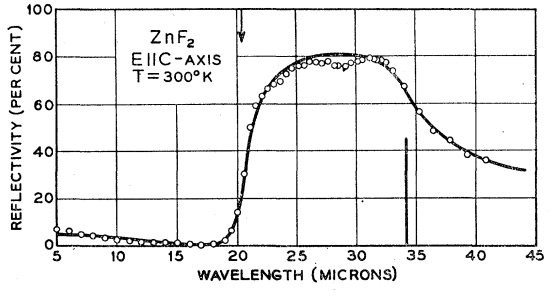

FIG. 4. Reflectivity of ZnF_2 for E parallel to the c axis. The solid curve is given by classical oscillator dispersion theory.

[7] W. G. Spitzer, D. Kleinman, and D. Walsh, Phys. Rev. 113, 127 (1959).

[8] M. Born, and K. Huang, *Dynamical Theory of Crystal Lattices* (Clarendon Press, Oxford, England, 1954), Sec. 8.

[9] We have included the square root of the appropriate reduced mass and of the unit cell volume in the definition of W to yield equations where mass does not appear explicitly. In these equations the damping and charge coefficients have dimensions of frequency.

[10] In a real crystal, γ must be frequency-dependent and have both real and imaginary parts which obey the Kramers–Kronig relation [M. Lax, Phys. Chem. Solids 25, 487 (1964)]. Probably the most important deviation from the constant γ chosen here occurs at high frequencies where the losses in a real crystal fall off much more rapidly than is consistent with constant γ. Such rapid falloff is usually not detectable in reflection experiments because it occurs in a frequency region where the real part of the dielectric constant rather than the imaginary part dominates the reflectivity equations. We may reproduce the essential features of this fall off by using $\mathrm{Re}(\gamma)=$const up to some frequency ω_0 well above the optic mode resonance. We then attach a truncating function $\mathrm{Re}(\gamma)\sim1/\omega$ or $\exp(-\omega/\omega_0)$ for frequencies above ω_0. The result is that to a good approximation we can still use a real and constant γ in all our equations for frequencies below ω_0; however, the restoring force parameter ω_1^2 now contains a frequency-independent contribution arising from the imaginary part of γ.

[11] We may show that $\alpha_j=Z_j$ if we assume a fairly simple and obvious form for the free energy density in the crystal. See Appendix 5 of Ref. 8.

$\omega_j\gamma_jZ_j\alpha_j$ coefficients, one set for vibrations along the a axis and one for vibrations along the c axis. We try plane-wave solutions

$$P, E, W_1, \cdots, W_n \sim e^{i(\omega t-kx)}. \tag{3}$$

On substitution of these solutions into Eq. (1), the mode amplitudes W_j are obtained. Substitituion of the W_j into Eq. (2) gives

$$P=\left[\sum_j \frac{\alpha_j Z_j}{\omega_j^2-\omega^2+i\omega\gamma_j}+\alpha_\infty\right]E. \tag{4}$$

The dielectric constant is immediately obtained as

$$\begin{aligned}\epsilon&=1+4\pi P/E\\&=\epsilon_\infty+\sum_j \frac{S_j\omega_j^2}{\omega_j^2-\omega^2+i\omega\gamma_j},\end{aligned} \tag{5}$$

i.e., the usual classical oscillator dispersion equation. $\epsilon_\infty=1+4\pi\alpha_\infty$ is introduced to describe the high-frequency asymptotic behavior of the dielectric constant. In addition we have introduced $S_j=4\pi\alpha_jZ_j/\omega_j^2$ as a convenient dimensionless mode strength. In terms of this mode strength, the low-frequency dielectric constant $\epsilon(0)$ is given by

$$\epsilon(0)=\epsilon_\infty+\sum_j S_j. \tag{6}$$

The dielectric constant ϵ merely gives the ratio of displacement D to electric field E for plane waves of arbitrary ω and k. k or ω or both may be complex since up to this point we have not restricted ourselves to free vibrations. By a suitable arrangement of charge and current sources, waves of arbitrary k and ω may of course be excited. We now solve for the free vibrations by insisting

$$\begin{aligned}\mathrm{div}D&=0=\mathrm{div}H,\\ \mathrm{Curl}E&=-\dot{H}/c,\\ \mathrm{Curl}H&=\dot{D}/c,\\ D&=E+4\pi P,\end{aligned} \tag{7}$$

that is, we remove all arbitrary sources (free currents and charge) from the medium. The first of the above equations $\mathrm{div}D=\epsilon\,\mathrm{div}E=0$ has two roots. If $\mathrm{div}E=0$, then the wave vector k is perpendicular to E (transverse modes); if $\epsilon=0$ then $\mathrm{div}E$ need not be zero and k turns out to be parallel to E (longitudinal modes) for the principal crystal directions being considered.

LONGITUDINAL SOLUTIONS

We start by studying the roots of $\epsilon=0$ in the case of n modes. It is convenient to multiply through Eq. (5) by all the resonant denominators and consider the roots of the following form:

$$\begin{aligned}&\epsilon\prod_{j=1}^{n}(\omega_j^2-\omega^2+i\omega\gamma_j)\\&=\omega_1^2\omega_2^2\cdots\omega_n^2(S_1+S_2\cdots+S_n+\epsilon_\infty)+i\omega(\cdots)\\&\quad-\omega^2(\cdots)-i\omega^3(\cdots)+\omega^4(\cdots)+i\omega^5(\cdots)-\cdots\\&\qquad+(-1)^n\omega^{2n}(\epsilon_\infty).\end{aligned} \tag{8}$$

The brackets containing dots represent different terms containing complicated combinations of S_j, ω_j, γ_j, and ϵ_∞.

Since the right side of Eq. (8) is a polynomial of degree $2n$, there are $2n$ roots to the equation $\epsilon=0$.[12,13] We will provisionally call these roots the longitudinal mode frequencies ω_{l_1}, ω_{l_2}, $\cdots\omega_{l_{2n}}$. From the form of the polynomial, we note that, when ω_l is a root, so is its negative complex conjugate $-\omega_l^*$. We may write the polynomial in its factored form:

$$\begin{aligned}&\epsilon\prod_j(\omega_j^2-\omega^2+i\omega\gamma_j)\\&\quad=(-1)^n\epsilon_\infty(\omega-\omega_{l_1})(\omega-\omega_{l_2})\cdots(\omega-\omega_{l_{2n}})\\&\quad=(-1)^n(\omega^2-|\omega_{l_1}|^2-2i\omega\,\mathrm{Im}(\omega_{l_1}))\cdots\\&\qquad\times(\omega^2-|\omega_{l_n}|^2-2i\omega\,\mathrm{Im}(\omega_{l_n})),\end{aligned} \tag{9}$$

where Im stands for "imaginary part of," and we have chosen the coefficient $(-1)^n\epsilon_\infty$ by inspection to give the correct leading term. We have also relabeled the roots in the third line making use of the way they occur in pairs and used $(\omega_l)\cdot(-\omega_l^*)=-|\omega_l|^2$. We obtain $2n-1$ sum rules by now equating coefficients of equivalent terms in Eqs. (8) and (9). The most important of these sum rules is the Lyddane-Sachs-Teller relation which comes from equating the constant term in each polynomial. Equating the constant terms on the right-hand sides of Eqs. (8) and (9) we obtain

$$\frac{|\omega_{l_1}|^2|\omega_{l_2}|^2|\omega_{l_3}|^2\cdots|\omega_{l_n}|^2}{\omega_1^2\omega_2^2\omega_3^2\cdots\omega_n^2}=\frac{\epsilon(0)}{\epsilon_\infty}. \tag{10}$$

This is the Lyddane-Sachs-Teller relation. It is interesting to note that for our model which includes damping, this Lyddane-Sachs-Teller relation connects the absolute value of the longitudinal mode frequencies with the force constant parameters ω_j. In the case of no damping, the ω_j will actually be the transverse mode frequencies, and the ω_{l_j} will be real allowing the absolute value signs to be dropped. Equation (10) then becomes identical in form of relations which have been derived by Cochran[14] and Kurosawa[15] from quite different considerations based on microscopic models.

---

[12] The resonant factors do not introduce any roots in addition to those of ϵ.

[13] The appearance of $2n$ roots in an n mode problem simply reflects a freedom in phase for each solution allowing us to specify both position and velocity as initial conditions.

[14] W. Cochran, Z. Krist. **112**, 465 (1959).

[15] T. Kurosawa, J. Phys. Soc. Japan **16**, 1298 (1961).

The coefficient of the ω^{2n} term gives no sum rule since this term was adjusted to scale the polynomial. The coefficient of the ω^{2n-1} term gives a sum rule on the γ_j's.

$$\gamma_1+\gamma_2+\cdots+\gamma_n=2(\mathrm{Im}(\omega_{l_1})+\mathrm{Im}(\omega_{l_2})+\cdots+\mathrm{Im}(\omega_{l_n})).$$

The coefficient of the ω^{2n-2} term gives a sum rule on the frequency weighted mode strengths $\omega_j^2 S_j$. The importance of these weighted strengths is their direct relation to the effective charge z_j [see discussion immediately below Eq. (5)]. Equating coefficients of the ω^{2n-2} term we obtain

$$\sum_j \omega_j^2 S_j=\sum_j(|\omega_{l_j}|^2-\omega_j^2).$$

This relation has been derived by Kurosawa[15] in the case of no damping. The remaining sum rules involve less useful combinations of the mode parameters and will not be given here.

For the case of one mode the sum rules are

$$\gamma_1=2\,\mathrm{Im}(\omega_{l_1}),$$

and

$$\frac{|\omega_{l_1}|^2}{\omega_1^2}=\frac{S_1+\epsilon_\infty}{\epsilon_\infty}=\frac{\epsilon(0)}{\epsilon_\infty}.$$

These relations are easily obtainable directly from the longitudinal root which can be written explicitly

$$\omega_l=\pm\left(\omega_1^2\left(\frac{S_1+\epsilon_\infty}{\epsilon_\infty}\right)-\frac{\gamma_1^2}{4}\right)^{1/2}+\frac{i\gamma_1}{2}.$$

To complete the discussion of the longitudinal solutions, we insert $\epsilon=0$ into Eq. (7) and find $H=0$, and that E, P, W, and k must all be parallel. The solutions are thus longitudinal modes with the frequencies given above and no k dependence (flat dispersion curves).

TRANSVERSE SOLUTIONS

For $\epsilon\neq 0$ Eqs. (7) permit transverse solutions with the k, E, and H vectors forming a right-handed system. The equations give the dispersion relation when E and H are eliminated between the two of Maxwell's equations involving the Curl. This relation is

$$k^2c^2/\omega^2=\epsilon, \tag{11}$$

where ϵ is given by Eq. (5). If the square root of ϵ is defined as the complex index of refraction, then Eq. (10) states the familiar result that the phase velocity of the transverse waves is determined by the index of refraction in the customary way. There are nontrivial wave vector dependences for these transverse modes. We will briefly examine the dispersion curve of the transverse modes for real frequencies since this gives a picture of the wave behavior in a dielectric during the usual infrared experiment. Figure 5 illustrates the transverse solutions for the three classical modes which

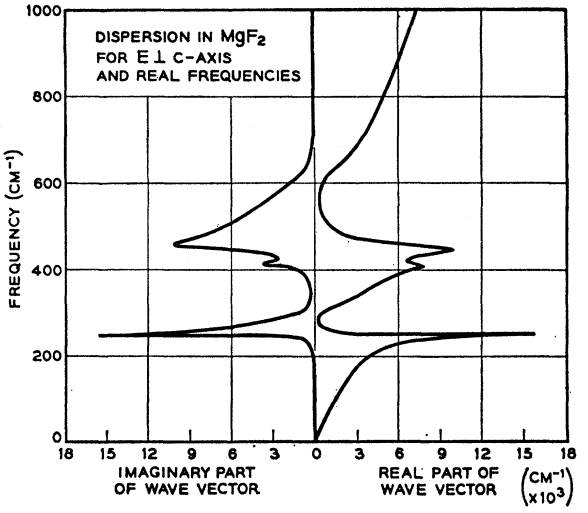

FIG. 5. Dispersion curves for the transverse modes in MgF_2 with E perpendicular to the c axis and for real frequency.

fit the c-axis dielectric behavior of MgF_2. The curves show the usual regions of photon-like behavior at very low and very high frequencies [with slopes determined by $\epsilon(0)$ and ϵ_∞, respectively] continuously joining horizontal phonon-like curves. The quanta associated with such mixed phonon-photon curves are sometimes called polaritons.

We *define* the transverse phonon frequencies as ω_{t_j}, the poles of the dielectric constant given by

$$\omega_{t_j}=\pm(\omega_j^2-\gamma_{j/4}^2)^{1/2}+i\gamma_{j/2}. \tag{12}$$

We note, however, that transverse vibration modes exist at all frequencies. Born and Huang have given an excellent discussion of the dispersion curves in the case of a single undamped mode.[8] They point out that for such phonon dispersion curves, as the wave vector k increases, energy is carried more and more predominantly by the elastic rather than the electromagnetic part of the field. The definition chosen above [Eq. (12)] for the transverse optic phonon mode frequency corresponds to the limit of large k, where the ratio of mechanical to electric field amplitude has become infinite. As mentioned earlier, we note that the phonon frequency is shifted from the restoring force value ω_j when there is damping present. The limiting behavior where the dispersion curves approach the phonon frequency is only partially shown in Fig. 5 since this figure is drawn for real frequencies.

EXPERIMENTAL DETERMINATION OF FREQUENCIES

For discussing most infrared experiments we may restrict the frequency to be real. If the dielectric constant function for real frequencies can be determined (for instance by fitting the reflectivity), then the constants ω_j, γ_j, S_j, and ϵ_∞ can be determined and

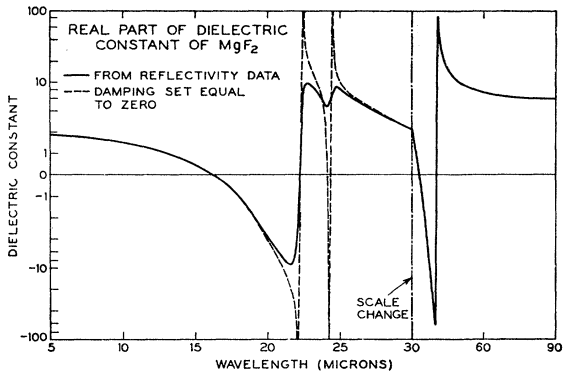

FIG. 6. Real part of ϵ for MgF_2 ($E \perp c$ axis). The dashed curve results when the damping of the two higher frequency modes is reduced to zero. This curve is used to determine the longitudinal phonon frequencies.

any of the above complex frequencies can be evaluated. Roughly speaking, for thick samples with well-spaced lightly damped modes, the high- and low-frequency edges of the restrahlen band fall at the real part of the longitudinal and transverse phonon frequencies. In transmission experiments with thin samples, absorption lines are obtained at both the longitudinal and transverse phonon frequencies if non-normal incidence is used.[16] Figures 1 to 4 show the transverse and longitudinal mode frequencies in MgF_2 and ZnF_2 along with the reflectivity for comparison. These frequencies are determined as follows. In the present work, γ_j is at most 9% of ω_j, and reflectivity fitting can be carried out to an accuracy of about 1% in frequency. Therefore, terms like $\gamma_{j/4}{}^2$ can be neglected compared with $\omega_j{}^2$ in most of the formulas. The procedure has been adopted therefore of quoting the parameters ω_j which produced the best reflectivity fit, as the transverse phonon frequencies. Next the zeros of ϵ' (the real part of ϵ) along the real frequency axis are determined. Alternate zeros are discarded since along the real frequency axis ϵ' has extra zeros from a factor $(\omega_j{}^2-\omega^2)$ in the numerator. The remaining zeros are adopted as the longitudinal phonon frequencies. If ϵ' does not have zeros (for real frequency) corresponding to some of the longitudinal modes, the damping can be set equal to zero in Eq. (5) and the real part of ϵ can be recalculated. Zeros now appear which approximate the real part of the longitudinal phonon frequencies within the accuracies stated above. Figure 6 shows the real part of ϵ for MgF_2 and the changes that result when the damping of the two highest frequency modes is reduced to zero. We note that two new zeros appear and that the other zeros are not shifted. According to our procedure, the lower frequency zero of this pair is to be discarded and the higher frequency zero designated ω_{l_2}. Table I gives all the optic mode phonon frequencies for MgF_2 and ZnF_2 deduced in the manner just described. Comparison of Table I with the work of Johnson *et al.* shows that none of the phonons observed here could be associated with the laser action by a one-phonon process. Since the MgF_2 fluorescence spectrum[1] probably reflects a one-phonon density of states, we might look for comparisons with the forbidden mode seen in MgF_2 at 556 cm^{-1} in the present work. It appears likely that this forbidden mode is a sum band involving phonons seen in fluorescence at about 6164 and 6300 cm^{-1}, i.e., phonons with frequencies 338 and 200 cm^{-1}. If the optic branches are fairly flat across the Brillouin zone in MgF_2, the 556 cm^{-1} forbidden mode might also be due to the 410 or 415 cm^{-1} optic modes combining with the 155-cm^{-1} phonons seen in fluorescence.

The low-frequency dielectric constant $\epsilon(0)$ may be predicted from the mode strengths and the high-frequency dielectric constant obtained in the present study. Table I gives $\epsilon(0)$ for the electric vector parallel and perpendicular to the c axis for MgF_2 and ZnF_2.

CONCLUSION

The eight infrared mode frequencies in MgF_2 and in ZnF_2 have been evaluated from reflectivity data. Four of these modes are the usual "infrared active" or transverse phonon modes and four are the associated longitudinal phonon modes split off by the Coulomb interaction. Though the transverse modes usually determine absorption (see, however, Ref. 16), the longitudinal modes determine important features of the dielectric constant and are easily obtained from an analysis of reflectivity measurements. A general Lyddane-Sachs-Teller relation has been derived which reduces to the form given by others in the case of zero damping. Additional "sum rules" connecting mode parameters and the phonon frequencies are derived in a systematic way. The low- and high-frequency dielectric constants are deduced for the principle directions in MgF_2 and ZnF_2. It is to be emphasized that in infrared experiments where there is appreciable damping any frequency associated with a physical effect must be defined quite carefully relative to the theory used to describe the dispersion. A simple example is provided by the classical oscillator with one mode. While the imaginary part of the dielectric constant ϵ'' is often plotted to show the mode structure, it is known that the maximum in ϵ'' does not occur at the frequency ω_1. The maximum of the real part of the conductivity however, occurs exactly at ω_1 for any value of damping. Thus the conductivity curve may be used to determine ω_1 directly. The point being stressed here is that once ω_1 is determined it must be recognized as only a parameter of the theory, not as a phonon frequency, if accuracies of order γ_1/ω_1 are important.

[16] D. W. Berreman, Phys. Rev. **130**, 2193 (1963).